INTERNATIONAL JOURNAL FOR NUMERICAL METHODS IN FLUIDS
Int. J. Numer. Meth. Fluids 2004; **45**:659–688 (DOI: 10.1002/fld.722)

A combined analytical–numerical method for treating corner singularities in viscous flow predictions

J.-M. Shi[‡,§], M. Breuer[*,†] and F. Durst

Institute of Fluid Mechanics, University of Erlangen-Nürnberg, Cauerstr. 4, D-91058 Erlangen, Germany

SUMMARY

A combined analytical–numerical method based on a matching asymptotic algorithm is proposed for treating angular (sharp corner or wedge) singularities in the numerical solution of the Navier–Stokes equations. We adopt an asymptotic solution for the local flow around the angular points based on the Stokes flow approximation and a numerical solution for the global flow outside the singular regions using a finite-volume method. The coefficients involved in the analytical solution are iteratively updated by matching both solutions in a small region where the Stokes flow approximation holds. Moreover, an error analysis is derived for this method, which serves as a guideline for the practical implementation. The present method is applied to treat the leading-edge singularity of a semi-infinite plate. The effect of various influencing factors related to the implementation are evaluated with the help of numerical experiments. The investigation showed that the accuracy of the numerical solution for the flow around the leading edge can be significantly improved with the present method. The results of the numerical experiments support the error analysis and show the desired properties of the new algorithm, i.e. accuracy, robustness and efficiency. Based on the numerical results for the leading-edge singularity, the validity of various classical approximate models for the flow, such as the Stokes approximation, the inviscid flow model and the boundary layer theory of varying orders are examined. Although the methodology proposed was evaluated for the leading-edge problem, it is generally applicable to all kinds of angular singularities and all kinds of finite-discretization methods. Copyright © 2004 John Wiley & Sons, Ltd.

KEY WORDS: combined analytical–numerical method; matching asymptotic algorithm; angular singularities; Navier–Stokes equations; Stokes approximation; accuracy; robustness; efficiency; leading edge

1. INTRODUCTION

It is well known that the presence of angular points (sharp edge or corners) within computational domains can cause serious errors in viscous flow simulations if a standard finite

[*]Correspondence to: M. Breuer, LSTM, Universität Erlangen-Nürnberg, Cauerstr. 4, D-91058 Erlangen, Germany.
[†]E-mail: breuer@lstm.uni-erlangen.de
[‡]E-mail: j.shi@fz-rossendorf.de
[§]Present address: Institute for Safety Research, Research Center Rossendorf, Bautzner Landstr. 128, 01328 Dresden, Germany.

Contract/grant sponsor: FORTWIHR
Contract/grant sponsor: KONWIHR

Published online 8 April 2004

Received 21 June 2003
Revised 22 January 2004

discretization scheme is applied. The reason is that the exact solution of an elliptic equation, e.g. the pressure, vorticity and shear stress, can be singular at angular points [1–5]. Hence, the numerical solution of these quantities diverge in the singular region, which not only causes additional (local or non-local) numerical errors, but also degrades the rate of convergence (non-local) or even leads to divergence of the entire numerical solution [4, 6, 7].

Various methods have been proposed or adopted in practice in order to improve the numerical accuracy for problems involving angular singularities. One of them is the conformal transformation. For example, Botta and Dijkstra [8] successfully applied this technique to treat the leading-edge singularity of a semi-infinite plate. Nevertheless, a suitable transformation is not always available in practice. Moreover, the transformation sometimes results in ill-conditioned matrices of the discrete equations. As a result, the numerical accuracy and convergence can be bad. Other methods that are not limited to some specific geometries can either be classified into *purely numerical treatments* or *combined analytical–numerical methods*. Examples of the former include the local modification of the differencing scheme or boundary condition [9–11], special extrapolation around re-entrant corners [12], local grid refinement [13, 14] and adaptive and optimal grid methods [15, 16]. These methods except for those ad hoc treatments given in Reference [9] are useful in improving the global numerical accuracy in many cases where the numerical pollution arising from an angular singularity is locally bounded. Nevertheless, the error has a non-local character for the anti-symmetrical part of the solution of the Navier–Stokes equations [17], especially when strong convection is present [12]. Moreover, considering the limitation of the finite arithmetic in the approximation of singularities, the numerical results will become progressively worse if the singular locations are approached. Hence, these methods are not suitable if one is interested in the flow in the vicinity of sharp corners or wedges.

As mentioned above an alternative to a purely numerical treatment are *combined analytical–numerical methods* requiring appropriate analytical solutions for the vicinity of the singularity. Asymptotic solutions can be obtained for the local viscous flow around an angular point under the Stokes flow approximation [2, 3]. To solve viscous flows near an angular point accurately, a useful method is to incorporate the local solution in the numerical scheme. One of the examples is the singular element method whose shape functions are based on the local analysis. This method was applied to treat the stress singularity in die swell problems in Stokes flows [6, 7, 18]. Several studies [17, 19, 20] have employed the local asymptotic solution for the Stokes flow to overcome the vorticity singularity in the numerical solution of the Navier–Stokes equations adopting the stream function-vorticity formulation. They assigned the local asymptotic solution for the Stokes flow in the neighbourhood of an angular point as the boundary condition for the flow in the remaining region, which was solved using a finite-difference scheme. An iterative matching procedure was adopted between both solutions and the coefficients involved in the local solution were iteratively updated. However, the convergence of the numerical solution using this strategy strongly depends on the implementation. For example, Ingham *et al.* [19] assigned the local solution to three grid points closest to the tip of a vertical flat plate and determined the unknown coefficients of the local solution from the numerical solution at the adjacent points. They reported that a very small under-relaxation factor has to be applied in order to achieve convergence. In *et al.* [20] considered the same problem. They introduced a sub-zone matching procedure rather than the point matching as in Reference [19] and achieved robust convergence. The accuracy of the numerical solution was not reported in both studies. Furthermore, the authors did not perform any analysis of the grid size effect

or the influences of several factors related to the implementation, e.g. the number of grid points assigned to the analytical solution or involved in the matching procedure, the location of these points, the matching strategy (point matching or zone matching), and the order of the local expansion. Partly these influences are demonstrated by the grid convergence study of Floryan and Czechowsky [17]. Based on their numerical experiments and a failed test case, the authors concluded that one must be cautious in using the combined analytical–numerical strategy, despite the fact that it is well-founded theoretically. Nevertheless, neither this work nor the other studies known to us can tell how accurate the numerical solution based on the combined analytical–numerical strategy can be, how to achieve good accuracy, convergence and efficiency, how much can the implementation affect them or what implementation might be optimal in accuracy and robustness. Hence in the present work efforts were made to clarify the above questions.

Presently, we propose a *combined analytical–numerical strategy* for treating the pressure and shear stress singularities in the framework of the *primitive variable formulation* of the Navier–Stokes equations and using a *finite-volume discretization* for the numerical solution. The primitive variable method is of advantage over the stream function-vorticity approach for the possibility of a direct extension to three-dimensional problems though few work except for that by Ladevèze and Peyret [21] has explored such a treatment. A formal error analysis was derived for the method proposed, which shows that the accuracy of the numerical solution in the critical region can be significantly improved by the *combined analytical–numerical strategy*. This analysis can also serve as a guideline for the practical implementation. We applied this method to treat the leading-edge singularity in a laminar flow over a semi-infinite plate. This problem is of fundamental interest in developing the boundary layer theory. It is well known that the classical Prandtl–Blasius solution or the higher-order boundary layer theories represent asymptotic solutions for high Reynolds number, $Re_x = Ux/v \gg 1$, where x is the running length starting from the leading edge. Thus, they are not expected to be valid near the leading edge where $Re_x \sim O(1)$. As is discussed in detail in Reference [22], the flow close to the leading edge remains unsolved with purely analytical approaches despite a lot of efforts. The only result that can be obtained is the local asymptotic solution for $Re_r \to 0$ where r is the radial distance from the singular point [1], which contains coefficients depending on the remote flow outside the range of validity of the local expansion. With the present method, we obtained an accurate solution for the flow of interest. Furthermore, systematic numerical experiments were performed and the effect of various influencing factors related to the implementation were evaluated in detail. The results of the numerical experiments support the error analysis and show the desired properties of the new algorithm, i.e. accuracy, robustness and efficiency. Based on the numerical results, the validity of various classical approximate models for the flow close to the leading edge such as the Stokes approximation, the inviscid flow model and the boundary layer theory of varying orders were examined.

2. THEORETICAL MODEL

2.1. Governing equations

Although the present treatment for angular singularities is generally applicable, it is convenient to describe it based on a specific problem. Let us consider the two-dimensional, steady and

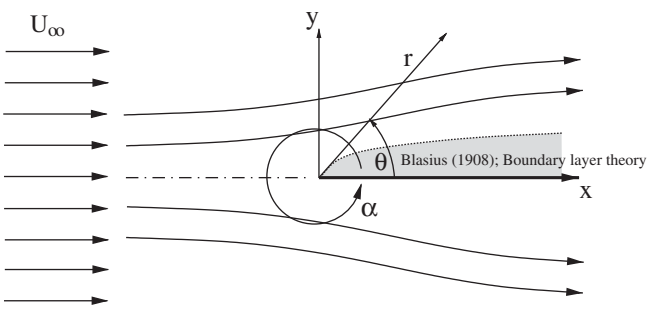

Figure 1. Schematic diagram of the viscous flow around the leading edge of a semi-infinite plate.

laminar flow of an incompressible Newtonian fluid over a parallel, semi-infinite flat plate of vanishing thickness (see Figure 1), the governing equations (Navier–Stokes equations) can be written in the following non-dimensional form,

$$\nabla^* \cdot \tilde{\mathbf{U}}^* = 0 \tag{1}$$

$$\nabla^* \cdot (\tilde{\mathbf{U}}^* \tilde{\mathbf{U}}^*) = -\nabla^* P^* + \nabla^{*2} \tilde{\mathbf{U}}^* \tag{2}$$

where

$$\tilde{\mathbf{U}}^* = \frac{\tilde{\mathbf{U}}}{U_\infty}, \quad P^* = \frac{P - P_\infty}{\rho U_\infty^2} \tag{3}$$

are the velocity vector and the pressure, respectively. The free-stream velocity $U_c = U_\infty$ and the diffusion length scale $\ell_c = \nu / U_\infty$ are used as characteristic quantities for the normalization. As a result, one gets $Re = (U_c \ell_c / \nu) = 1$. In addition, the dimensionless co-ordinates have the physical meaning of a local Reynolds number, i.e. $x^* = Re_x$ and $y^* = Re_y$.

2.2. *Local expansion around the leading edge*

In the vicinity of a sharp wedge or corner where the inertia force is small compared with the viscous effect, namely

$$\frac{\|\tilde{\mathbf{U}}^* \cdot \nabla^* \tilde{\mathbf{U}}^*\|}{\|\nabla^{*2} \tilde{\mathbf{U}}^*\|} \ll 1 \tag{4}$$

the Stokes approximation can be applied. Hence, the momentum equation (2) reduce to

$$\nabla^{*2} \tilde{\mathbf{U}}^* = \nabla^* P^* \tag{5}$$

Applying the **curl** operator $(\nabla^* \times)$ to Equation (5), one obtains a Laplace equation for the vorticity $\omega^* = (\nabla^* \times \tilde{U}^*)_z$

$$\nabla^{*2} \omega^* = 0 \tag{6}$$

Substituting Equation (6) into the stream-function equation of a Navier–Stokes flow, i.e.

$$\nabla^{*2}\psi^* = -\omega^* \tag{7}$$

leads to the biharmonic equation for the stream function ψ^*:

$$\nabla^{*4}\psi^* = 0 \tag{8}$$

where ψ^* and ω^* are normalized as $\psi^* = \psi/\nu$ and $\omega^* = \omega\nu/U_\infty^2$.

Adopting the polar co-ordinate system (r^*, θ) (see Figure 1), the no-slip boundary conditions at the wall are

$$u_r^* = \frac{1}{r^*}\frac{\partial\psi^*}{\partial\theta} = 0 \quad \text{and} \quad u_\theta^* = -\frac{\partial\psi^*}{\partial r^*} = 0, \quad \text{when } \theta = 0, 2\pi \tag{9}$$

Following Moffat [2], Equation (8) permits an asymptotic solution by using the eigenvalue expansion:

$$\psi^*(r^*, \theta) = \psi_0^* + \sum_{i=1}^{n} A_{\lambda_i} r^{*\lambda_i+1} f_{\lambda_i}(\theta) + \mathbf{O}(r^{*\lambda_{n+1}+1}) \tag{10}$$

where r^* is the dimensionless distance from the leading edge and $\lambda_i < \lambda_{i+1}$ are the eigenvalues, which are *real* numbers as required for physical flows. The eigenvalues are determined by the boundary conditions at the wall, i.e. Equation (9). Thus they are functions of the angle at the corner, α ($= 2\pi$ for the leading edge problem). Finite velocities at the leading edge require that the smallest eigenvalue λ_1 has to be positive. In addition, since the leading-order term is dominant, in view of Equation (4) the Stokes approximation is valid only when

$$Re_{\text{local}} = \frac{\|\tilde{\mathbf{U}}^* \cdot \nabla^* \tilde{\mathbf{U}}^*\|}{\|\nabla^{*2}\tilde{\mathbf{U}}^*\|} \approx |A_{\lambda_1}|\, r^{*\lambda_1+1} \ll 1 \tag{11}$$

Substituting Equation (10) into Equation (8), one obtains the following equation for the function $f_{\lambda_i}(\theta)$ in the case $\lambda_i \notin \{-1, 0, 1\}$,

$$f_{\lambda_i}^{(4)}(\theta) + [(\lambda_i - 1)^2 + (\lambda_i + 1)^2] f_{\lambda_i}''(\theta) + (\lambda_i + 1)^2(\lambda_i - 1)^2 f_{\lambda_i}(\theta) = 0 \tag{12}$$

Correspondingly, the following boundary conditions can be derived from Equation (9) for $f_{\lambda_i}(\theta)$:

$$f_{\lambda_i}'(\theta) = 0 \quad \text{and} \quad f_{\lambda_i}(\theta) = 0, \quad \text{when } \theta = 0, \alpha \tag{13}$$

Under the condition of the present study that the flow is symmetrical with respect to the x-axis, the solution of this equation is given by symmetrical bases:

$$f_{\lambda_i}(\theta) = f_{\lambda_i}^{\text{s}}(\theta) \in \{\sin[(\lambda_i + 1)(\pi - \theta)], \sin[(\lambda_i - 1)(\pi - \theta)]\} \tag{14}$$

which additionally satisfies the conditions $f_{\lambda_i}^{\text{s}}(\pi) = 0$ and $f_{\lambda_i}^{\text{s}\prime}(\pi) = 0$. A general solution procedure of the biharmonic Equation (12) with the boundary conditions (13) leads to the following result for an eigenvalue:

$$\sin(\lambda\alpha) = \pm\lambda \sin(\alpha) \tag{15}$$

where λ is a positive real root of Equation (15), as required for the physical flow. Substituting $\alpha = 2\pi$ into Equation (15), one has $\lambda = k/2$, where k is a positive integer.

With the additional symmetry condition of the flow mentioned above, the eigenvalues can be finally determined for the Stokes flow around the leading edge of a semi-infinite flat plate in a parallel free stream. A detailed solution procedure of the problem is given in Reference [23]. Here we provide the solutions for the Cartesian velocity components and the pressure, which were employed for the numerical solution:

$$\begin{aligned} U^* = {} & A_1 r^{*1/2}[\tfrac{1}{2}\sin(\tfrac{3}{2}\theta) + \tfrac{5}{2}\sin(\tfrac{1}{2}\theta)] \\ & + A_2 r^{*3/2}[\tfrac{7}{2}\sin(\tfrac{3}{2}\theta) + \tfrac{3}{2}\sin(\tfrac{1}{2}\theta)] \\ & + A_3 r^{*2}[6\cos(2\theta) - 6] \\ & + A_4 r^{*5/2}[\tfrac{9}{2}\sin(\tfrac{5}{2}\theta) - \tfrac{5}{2}\sin(\tfrac{1}{2}\theta)] \\ & + A_5 r^{*3}[6\cos(3\theta) - 6\cos(\theta)] \\ & + A_6 r^{*7/2}[\tfrac{7}{2}\sin(\tfrac{3}{2}\theta) - \tfrac{11}{2}\sin(\tfrac{7}{2}\theta)] + \cdots \end{aligned} \tag{16}$$

$$\begin{aligned} V^* = {} & A_1 r^{*1/2}[\tfrac{1}{2}\cos(\tfrac{1}{2}\theta) - \tfrac{1}{2}\cos(\tfrac{3}{2}\theta)] \\ & + A_2 r^{*3/2}[-\tfrac{3}{2}\cos(\tfrac{1}{2}\theta) + \tfrac{3}{2}\cos(\tfrac{3}{2}\theta)] \\ & + A_4 r^{*5/2}[\tfrac{5}{2}\cos(\tfrac{5}{2}\theta) - \tfrac{5}{2}\cos(\tfrac{1}{2}\theta)] \\ & + A_5 r^{*3}[-2\sin(3\theta) + 6\sin(\theta)] \\ & + A_6 r^{*7/2}[\tfrac{7}{2}\cos(\tfrac{3}{2}\theta) - \tfrac{7}{2}\cos(\tfrac{7}{2}\theta)] + \cdots \end{aligned} \tag{17}$$

where the term with r^{*2} vanishes in Equation (17).

$$\begin{aligned} P^* = {} & 2A_1 r^{*-1/2}\sin(\tfrac{1}{2}\theta) - 6A_2 r^{*1/2}\sin(\tfrac{1}{2}\theta) \\ & - 24A_3 r^*\cos(\theta) - 10A_4 r^{*3/2}\sin(\tfrac{3}{2}\theta) \\ & - 24A_5 r^{*2}\cos(2\theta) + 14A_6 r^{*5/2}\sin(\tfrac{5}{2}\theta) + p_0 + \cdots \end{aligned} \tag{18}$$

where p_0 is a constant depending on the reference pressure of the free stream. Equation (18) shows that the pressure is singular at the leading edge with the order $r^{*-1/2}$. A singularity of the same order can also be expected in the vorticity ω^*, the shear stress $\tau^*_{r\theta}$, and the local skin friction (drag coefficient) of the plate, which is defined as

$$c_f = \frac{\tau_w(x^*)}{\frac{1}{2}\rho U_\infty^2} = 2\tau_w^*(x^*) = 2\,\frac{\partial U^*}{\partial y^*} \tag{19}$$

Substituting Equation (16) into Equation (19), one has

$$c_f = 4A_1 Re_x^{-1/2} + 12A_2 Re_x^{1/2} + 20A_4 Re_x^{3/2} - 28A_6 Re_x^{5/2} + \cdots \tag{20}$$

where $Re_x = x^*$ as shown above. The coefficients $A_i = A_{\lambda_i}$, $(i = 1, 6)$ remain unknown from the analysis. They have to be determined by matching the *local analytical solution* (Stokes equations) to the *numerical solution* of the outer flow (Navier–Stokes equations) in the neighbourhood of the leading edge where the Stokes approximation still holds.

3. COMBINED ANALYTICAL–NUMERICAL METHOD

With the help of the local solution, a combined numerical–analytical method based on the computational matching asymptotic strategy can be constructed. As sketched in Figure 2, the computational domain is decomposed into three parts, denoted by *Stokes region* (A), *matching region* (B) and *Navier–Stokes region* (C). The Stokes approximation is assumed to hold in both regions A and B. Hence the required condition (11) has to be satisfied in both regions. The asymptotic solutions (16)–(18) involving unknown coefficients is prescribed in the *Stokes region* (A) for the primitive variables (U^*, V^* and P^*) of the governing Equations (1) and (2). A finite-volume scheme as described in Section 4 is applied for the numerical solution of the flow in the rest of the computational domain (B and C). Since the Stokes approximation holds in the flow region B, solutions (16)–(18) obtained from the local analysis are expected to match the numerical solution of the Navier–Stokes equations in this region. As a result, the unknown coefficients involved in the local asymptotic solutions (16)–(18) can be determined.

The least-square method is employed to calculate the unknown coefficients. Without loss of generality, the local solution for a dependent variable can be expressed as

$$\phi^{\text{anal}}(r_i^*, \theta_i) = c_0 + \sum_{k=1}^{m} A_{\lambda_k} g_{\lambda_k}(r_i^*, \theta_i) + \cdots \tag{21}$$

where c_0 is employed to represent a constant and $g_{\lambda_k}(r_i^*, \theta_i)$ is a representative for the functions appearing in Equations (16)–(18). Matching this solution to the corresponding value

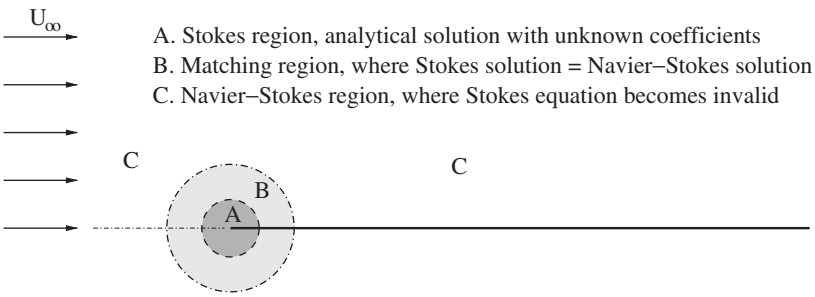

Figure 2. A sketch of the decomposition of the computational domain for the matching asymptotic solution.

computed from the global numerical scheme, $\phi^{\text{num}}(r_i^*, \theta_i)$, leads to the following equation:

$$c_0 + \sum_{k=1}^{m} A_{\lambda_k} g_{\lambda_k}(r_i^*, \theta_i) = \phi^{\text{num}}(r_i^*, \theta_i), \quad i = 1 \ldots n \tag{22}$$

where i and n are the indices and the total number of the control volumes involved in the matching procedure, respectively.

Equation (22) can be expressed in a matrix form:

$$\mathbf{B}_{\mathbf{n},\mathbf{m}} \mathbf{A}_{\mathbf{m}} = \mathbf{G}_{\mathbf{n}} \tag{23}$$

where $\mathbf{A} = (A_{\lambda_1}, A_{\lambda_2}, \ldots, A_{\lambda_m})^{\mathrm{T}}$ is the unknown matrix, $\mathbf{B}$ is defined by $B_{i,k} = g_{\lambda_k}(r_i^*, \theta_i)$, and $\mathbf{G} = (\phi^{\text{num}}(r_1^*, \theta_1) - c_0, \phi^{\text{num}}(r_2^*, \theta_2) - c_0, \ldots, \phi^{\text{num}}(r_n^*, \theta_n) - c_0)^{\mathrm{T}}$.

Multiplying both sides of Equation (23) with $\mathbf{B}^{\mathrm{T}}$ from the left leads to the following equation for the unknown coefficients:

$$\mathbf{C}_{\mathbf{m},\mathbf{m}} \mathbf{A}_{\mathbf{m}} = \mathbf{D}_{\mathbf{m}} \tag{24}$$

where

$$\mathbf{C}_{\mathbf{m},\mathbf{m}} = \mathbf{B}^{\mathrm{T}}_{\mathbf{n},\mathbf{m}} \mathbf{B}_{\mathbf{n},\mathbf{m}} \quad \text{or} \quad C_{j,k} = \sum_{i=1}^{n} g_{\lambda_j}(r_i^*, \theta_i) g_{\lambda_k}(r_i^*, \theta_i) \tag{25}$$

and

$$\mathbf{D}_{\mathbf{m}} = \mathbf{B}^{\mathrm{T}}_{\mathbf{n},\mathbf{m}} \mathbf{G}_{\mathbf{n}} \quad \text{or} \quad D_j = \sum_{i=1}^{n} g_{\lambda_j}(r_i^*, \theta_i)[\phi^{\text{num}}(r_i^*, \theta_i) - c_0] \tag{26}$$

Equation (24) combined with Equations (25) and (26) is a formulation for the least-square calculation of the unknown coefficients involved in the local solution (21). Since $\mathbf{B}$ is known from the co-ordinates of the matching points and $\mathbf{G}$ from the global numerical solution, $\mathbf{C}$ and $\mathbf{D}$ can be calculated. Therefore, the coefficients of the local solution, A_{λ_k} $(k = 1, \ldots, m)$, can be determined by solving Equation (24). Then the constant c_0 can also be calculated using the same method:

$$c_0 = \frac{1}{n} \sum_{i=1}^{n} \left[\phi^{\text{num}}(r_i^*, \theta_i) - \sum_{k=1}^{m} A_{\lambda_k} g_{\lambda_k}(r_i^*, \theta_i) \right] \tag{27}$$

For the leading-edge problem, one has $c_0 = 0$ in Equation (21) if $\phi = U^*$ or V^*, considering the no-slip condition at the plate wall. Hence only $c_0 = p_0$ needs to be determined for the variable P^* [see Equation (18)]. This value is passive in the computation if U^* or V^* is chosen as the matching variable, since it does not have any influence on the results of A_{λ_k}. Only in the case when A_{λ_k} $(k = 1 \ldots m)$ are calculated from a matching procedure based on P^* does p_0 have an effect on the coefficients.

The matching procedure described above is incorporated in the iterative numerical algorithm for the global flow (refer to Section 4). Since the numerical scheme is not applied to region A, the local asymptotic solution prescribed there is equivalent to providing a boundary condition for the numerical solution of the remaining computational domain (B and C). Hence in the practical implementation, the local solution for the velocities (16) and (17) are applied only as boundary conditions at the interface between regions A and B, which can be called the *Stokes inlet*, rather than in the entire *Stokes region* (A). The coefficients and the prescribed

analytical boundary conditions at the Stokes inlet are updated at each outer iteration. The under-relaxation method is applied in the iterative calculation of the coefficients to ensure good convergence, which can be expressed as follows:

$$A_{\lambda_k}^{(l+1)} = A_{\lambda_k}^{(l)} + \alpha_\phi [A_{\lambda_k}^{(l+1)} - A_{\lambda_k}^{(l)}] \tag{28}$$

where l is the outer iteration number and α_ϕ is the under-relaxation factor corresponding to the dependent variables $\phi = U^*, V^*$ and P^*.

Total convergence, both for the numerical solution of the global flow (convergence criterion denoted by ε_{num}) and for the coefficients of the local solution (convergence criterion denoted by $\varepsilon_{\text{coeff}}$), is required before the numerical calculation stops. The local solution can be considered as converged if the relative changes of all coefficients during the iteration, namely

$$\varepsilon_{\text{coeff}} = \left\{ \varepsilon_{A_k} = \frac{|A_{\lambda_k}^{(l+1)} - A_{\lambda_k}^{(l)}|}{|A_{\lambda_k}^{(l)}| + \varepsilon},\ k = 1 \ldots m;\ \varepsilon_{p_0} = \frac{|p_0^{(l+1)} - p_0^{(l)}|}{|p_0^{(l)}| + \varepsilon} \right\} \tag{29}$$

decrease to certain small levels, where $\varepsilon = 10^{-20}$ is a negligible positive value to avoid zero denominators.

With the computational matching asymptotic strategy described above, the singularity at the leading edge is completely avoided in the global numerical scheme. In principle, various methods can be applied for the solution of Equation (24). However, an iterative Gauss–Seidel method is preferred considering the fact that the lower-order terms are more important than those of higher order. Numerical experiments indicate that the matching calculation is not sensitive to the choice of α_ϕ. A value between 0.5 and 1.0 usually leads to good convergence. In addition, calculations choosing U^* as the matching variable are found to provide the best results both in convergence and accuracy for the present problem, although the matching procedure can principally be based on each of the dependent variables or any combination of them. A detailed discussion on this topic is provided in Section 6.4.

As an alternative to the *least-square* matching, the *exact* matching strategy, which solves the same number of matching equations as the coefficients, namely $n = m+1$ in Equation (22), were applied in References [17, 19]. Nevertheless, we found that this method is not robust since the convergence speed and the results can be very sensitive to the matching locations.

4. FINITE-VOLUME FLOW SOLVER

The numerical solution of the Navier–Stokes equations is based on the finite-volume flow solver FASTEST-2D (see Reference [24]). The code employed a block-structured, boundary-fitted non-orthogonal quadrilateral grid and a colocated arrangement of the variables as described by Demirdžić and Perić [25]. The convection and diffusion contributions to the fluxes are evaluated using a central differencing scheme of second-order accuracy (CDS). For the convective part the CDS scheme is blended with the first-order upwind differencing scheme (UDS) using the deferred-correction approach proposed by Khosla and Rubin [26]. Linearization is introduced in the discretization and solution procedure for the Navier–Stokes equations. For the pressure calculation, a pressure-correction equation is derived from the continuity equation (1) and the momentum equations (2), which is iteratively solved together with the momentum equations following the SIMPLE algorithm proposed by Patankar and

Spalding [27]. An incomplete LU factorization method by Stone [28], called the strong implicit procedure (SIP), is used as the solver for the system of linearized algebraic equations. A non-linear multi-grid scheme is applied for convergence acceleration (see, e.g. Reference [29]). A local grid refinement technique [30] is employed to achieve high local resolution near the leading edge.

5. ERROR ANALYSIS

In the flow region A, where the Stokes approximation (5) applies, the convection term of the Navier–Stokes equations is negligible. Hence the discretization accuracy mainly depends on the discretization schemes for the diffusion term ($\nabla^{*2}\tilde{\mathbf{U}}^*$) and the pressure gradient ($\nabla^* P^*$). They are of second-order accuracy in space in the case of equidistant grids, as described in Section 4. Denoting the numerical solution by ϕ_h and the exact solution by ϕ, one has the following general expression:

$$\phi_h = \phi + d\phi_{\text{dis}} \quad \text{with } d\phi_{\text{dis}} = O(|\phi''|h^2) \tag{30}$$

where $d\phi_{\text{dis}}$ is the discretization error, h is the grid size and $|\phi''|$ represents the absolute value of the second-order derivative. Moreover, the relation between ϕ and the local asymptotic solution of the Stokes equations, denoted by ϕ_{anal}, can be written as follows:

$$\phi = \phi_{\text{anal}} + d\phi_{\text{exp}} + d\phi_{\text{eq}} \tag{31}$$

where $d\phi_{\text{exp}}$ represents the expansion error due to neglect of higher-order expansions and $d\phi_{\text{eq}}$ represents the approximate equation error introduced by the Stokes approximation of the Navier–Stokes equations, namely neglecting the convection term. Substituting Equation (31) into Equation (30) leads to the following general expression:

$$\phi_h = \phi_{\text{anal}} + d\phi_{\text{exp}} + d\phi_{\text{eq}} + d\phi_{\text{dis}} \tag{32}$$

With reference to Equations (16)–(18), an asymptotic expansion ϕ_{anal} up to the eigenvalue λ_m can be expressed as follows:

$$\phi_{\text{anal}} = \sum_{k=1}^{m} r_0^{*\lambda_k} f_{\lambda_k}^{\phi}(\theta) \quad \text{for } \phi = U^* \text{ and } V^* \tag{33}$$

$$\phi_{\text{anal}} = \sum_{k=1}^{m} r_0^{*\lambda_k - 1} f_{\lambda_k}^{\phi}(\theta) \quad \text{for } \phi = P^* \tag{34}$$

where (r_0^*, θ) are the polar co-ordinates at the centre of the CV under consideration. Hence the expansion error is obvious:

$$d\phi_{\text{exp}} = O(r_0^{*\lambda_{m+1}}),\ \phi = U^* \text{ and } V^*, \quad d\phi_{\text{exp}} = O(r_0^{*\lambda_{m+1}-1}),\ \phi = P^* \tag{35}$$

As a good approximation, $|\phi''|$ can be evaluated based on ϕ_{anal}. Hence we have

$$d\phi_{\text{dis}} \approx |\phi''_{\text{anal}}|h^2 = O(r_0^{*\lambda_1 - 2}h^2) \quad \text{for } \phi = U^*, V^* \tag{36}$$

$$d\phi_{\text{dis}} \approx |\phi''_{\text{anal}}|h^2 = O(r_0^{*\lambda_1 - 3}h^2) \quad \text{for } \phi = P^* \tag{37}$$

The approximate equation error $d\phi_{\text{eq}}$ can be estimated in the following way. Considering two sets of solutions, $(\tilde{\mathbf{U}}^*_{\mathbf{N}}, P^*_N)$ for the incompressible Navier–Stokes equations and $(\tilde{\mathbf{U}}^*_{\mathbf{S}}, P^*_S)$ for the Stokes approximation, $d\phi_{\text{eq}}$ is equal to $\tilde{\mathbf{U}}^*_{\mathbf{d}} = \tilde{\mathbf{U}}^*_{\mathbf{N}} - \tilde{\mathbf{U}}^*_{\mathbf{S}}$ for the velocity vector and $P^*_d = P^*_N - P^*_S$ for the pressure, respectively. Subtracting Equation (2) by Equation (5) leads to the following equation,

$$\tilde{\mathbf{U}}^*_{\mathbf{N}} \cdot \nabla^* \tilde{\mathbf{U}}^*_{\mathbf{N}} = -\nabla^* \mathbf{P}^*_{\mathbf{d}} + \nabla^{*2} \tilde{\mathbf{U}}^*_{\mathbf{d}} \tag{38}$$

In order to take the matching variable into account, we distinguish the N-S solutions between velocity matching $(\tilde{\mathbf{U}}^*_{\mathbf{U}}, P^*_U)$ and pressure matching $(\tilde{\mathbf{U}}^*_{\mathbf{P}}, P^*_P)$. In the former case one assumes $\tilde{\mathbf{U}}^*_{\mathbf{U}} = \tilde{\mathbf{U}}^*_{\mathbf{S}}$. Hence Equation (38) turns out to be

$$\nabla^*(\mathbf{P}^*_{\mathbf{U}} - \mathbf{P}^*_{\mathbf{S}}) = -\tilde{\mathbf{U}}^*_{\mathbf{S}} \cdot \nabla^* \tilde{\mathbf{U}}^*_{\mathbf{S}} \tag{39}$$

Or in a matching procedure based on P, namely assuming $P_P = P_S$, then one has

$$\nabla^{*2}(\tilde{\mathbf{U}}^*_{\mathbf{P}} - \tilde{\mathbf{U}}^*_{\mathbf{S}}) = \tilde{\mathbf{U}}^*_{\mathbf{P}} \cdot \nabla^* \tilde{\mathbf{U}}^*_{\mathbf{P}} \approx \tilde{\mathbf{U}}^*_{\mathbf{S}} \cdot \nabla^* \tilde{\mathbf{U}}^*_{\mathbf{S}} \tag{40}$$

Hence irrespective of the matching variable (if the Stokes solution is known), we obtain the following estimation for the order of the error due to the Stokes flow approximation:

$$\nabla^{*2} \tilde{\mathbf{U}}^*_{\mathbf{d}} \sim \nabla^* \mathbf{P}^*_{\mathbf{d}} \approx \tilde{\mathbf{U}}^*_{\mathbf{S}} \cdot \nabla^* \tilde{\mathbf{U}}^*_{\mathbf{S}} \tag{41}$$

As an approximation, $\tilde{\mathbf{U}}^*_{\mathbf{S}}$ in the above equations can be evaluated based on the asymptotic solution of the Stokes equations, ϕ_{anal}. Then the following estimation for the approximate equation error $d\phi_{\text{eq}}$ can be obtained:

$$d\phi_{\text{eq}} = O(r_0^{*2\lambda_1+1}), \quad \phi = U^* \text{ and } V^* \tag{42}$$

$$d\phi_{\text{eq}} = O(r_0^{*2\lambda_1}), \quad \phi = P^* \tag{43}$$

In practice, one has to determine the coefficients of the local expansion by the matching algorithm. Equations (42) and (43) indicate that the approximate equation error of the pressure is larger than that of the velocity field. Hence it is advantageous to determine the unknown coefficients of the Stokes flow expansion based on the velocity matching. A detailed discussion is given in Section 6.4.

Based on the above analysis, the general error expression (32) can be rewritten as

$$\phi_h = \phi_{\text{anal}} + O(\underbrace{r_0^{*\lambda_1-2} h^2}_{d\phi_{\text{dis}}}, \underbrace{r_0^{*2\lambda_1+1}}_{d\phi_{\text{eq}}}, \underbrace{r_0^{*\lambda_{m+1}}}_{d\phi_{\text{exp}}}), \quad \phi = U^* \text{ and } V^* \tag{44}$$

$$\phi_h = \phi_{\text{anal}} + O(\underbrace{r_0^{*\lambda_1-3} h^2}_{d\phi_{\text{dis}}}, \underbrace{r_0^{*2\lambda_1}}_{d\phi_{\text{eq}}}, \underbrace{r_0^{*\lambda_{m+1}-1}}_{d\phi_{\text{exp}}}), \quad \phi = P^* \tag{45}$$

where $\lambda_1 = \frac{1}{2}$ for the leading edge.

The above equations show that the accuracy of the numerical results depends on the radial distance of the matching location from the singular point r_0^*, the grid size h, and the leading-order eigenvalue λ_1, as well as the order of the local expansion λ_{m+1}. It is interesting to note from Equations (44) and (45) that even using a second-order accurate discretization, the numerical solution ϕ_h has a maximum accuracy of the order of $h^{1/2}$ for $\phi = U^*$ and V^* and diverges at an order of $h^{-1/2}$ for $\phi = P^*$ at the location $r_0^* = h$. For this reason, a numerical algorithm solely based on a finite-discretization scheme fails to produce an accurate solution in the region close to angular singularities if no special treatment as in the present study is applied. In comparison, the second-order accuracy of the finite-discretization scheme is preserved in the outer flow region where $r_0^{*\lambda_1 - 3} \leqslant C$ (C represents a constant).

The above analysis also indicates that the matching asymptotic algorithm loses its advantage with respect to the accuracy if the matching CVs are located very close to the angular point, i.e. $r_0^* \approx h$, as done in some previous studies. With reference to Equations (44) and (45), an optimal accuracy can be achieved for the numerical solution in the critical region by choosing matching locations (r_0^*) and the mesh size (h) such that the discretization error $d\phi_{\text{dis}}$ is of the same level as the approximate equation error $d\phi_{\text{eq}}$ while the condition of the Stokes approximation [Equation (11)] is to be satisfied. In addition, a local expansion leading to the same order of expansion error as $d\phi_{\text{eq}}$ can be recommended. Although higher-order coefficients can in principle be obtained from the matching solution, they are not accurate.

In order to make a quantitative evaluation of the accuracy of the numerical results from the matching asymptotic computation, a quantity called the matching residual δ_ϕ is introduced. It is defined as the mean-square deviation between ϕ_h and ϕ_{anal}, namely

$$\delta_\phi = \frac{1}{n} \sum_{i=1}^{n} [\phi_h(i) - \phi_{\text{anal}}(i)]^2 \tag{46}$$

where n is the number of the control points used for the residual evaluation and $\phi = U^*, V^*$ and P^*.

With reference to Equations (44) and (45), one has the following residual estimations:

$$\delta_{U,V} \sim O(r_0^{*2\lambda_1 - 4} h^4, r_0^{*4\lambda_1 + 2}, r_0^{*2\lambda_{m+1}}) \tag{47}$$

$$\delta_P \sim O(r_0^{*2\lambda_1 - 6} h^4, r_0^{*4\lambda_1}, r_0^{*2\lambda_{m+1} - 2}) \tag{48}$$

It is worth pointing out that the asymptotic solution ϕ_{anal} for the Stokes flow is used for the calculation of the matching residuals (47) and (48) due to the fact that the exact solution ϕ is unknown. Thus the discretization, expansion and approximate equation errors both at the control points and at the matching locations contribute to the matching residual. Nevertheless, since ϕ_{anal} is only involved in the matching asymptotic computation at the Stokes inlet and the matching locations, only this part of the expansion and approximate equation errors have an effect on the accuracy of the numerical results.

6. NUMERICAL EXPERIMENTS

A number of numerical experiments were carried out in order to make the matching asymptotic algorithm robust, reliable and to examine the accuracy. The effects of different factors of implementation such as the variable on which the matching procedure is based, the location and the number of matching points, the order of the local expansion, the differencing scheme, and the grid resolution were systematically investigated. Analyses were performed for the grid-convergence rate of the local solution based on the numerical results of the coefficients obtained at varying multi-grid levels. Most of the numerical experiments were performed using the UDS discretization (for the convection term) for the purpose of faster convergence. Nevertheless, the numerical results of the local flow were still found to have a second-order convergence rate (refer to Section 6.5). Test calculations using the CDS scheme (only at the finest grid level) were also carried out for comparison. The matching residual (46), which is a useful indicator for the accuracy of the matching asymptotic calculation, was evaluated over a control region (window).

Furthermore, the convergence speed was examined. In the numerical experiments, convergence was assumed to be satisfied when the change of the coefficients of the local solution decreased to $\varepsilon_{\text{coeff}} = \varepsilon_{A_k} < 5 \times 10^{-7}$ for $k = 1 - 3$ and $\varepsilon_{\text{coeff}} = \varepsilon_{A_k} < 5 \times 10^{-6}$ for $k > 3$ (refer to Equation (29)). Additionally, to assure convergence the maximum sum of the normalized absolute residuals in all equations ε_{num} within the numerical solution of the global flow has to be reduced by six orders of magnitude. These criteria were proved to be safe. The corresponding convergence history for a case applying a local solution containing six expansion terms (Equations (16) and (17)), choosing U^* as the matching variable, and applying region matching is displayed in Figure 3.

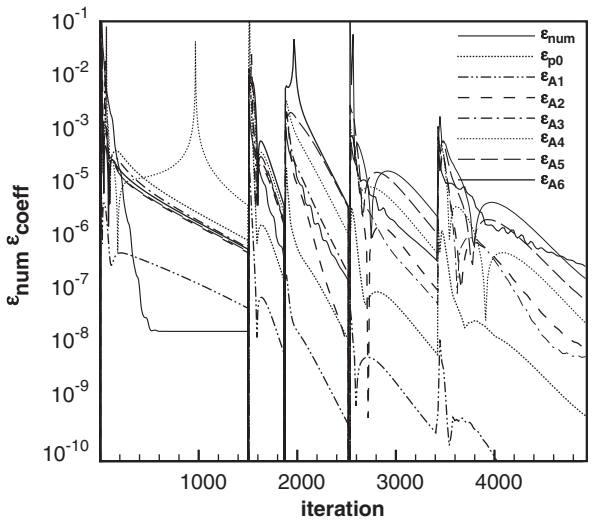

Figure 3. Convergence history of the numerical solution of the global flow ε_{num} and the coefficients of the local expansions $\varepsilon_{\text{coeff}}$ using region matching. The convergence criteria correspond to the values defined above.

Since the matching asymptotic algorithm is based on the iterative solution of the global flow, a jump is observed both for the change of the coefficients $\varepsilon_{\text{coeff}}$ and the residual of the global numerical solution ε_{num} at the shift of multi-grid levels during the computation. The relative change of the leading coefficient ε_{A_1} decreases most rapidly in all cases. This is an implied advantage of the sequential algorithm described in Section 3 and is ideal for a matching asymptotic calculation.

The numerical experiments served as a rigorous validation both for the matching asymptotic algorithm and for the error analysis of Section 5. Here only a small part of the results are presented. For a systematic presentation of all results from a complete set of test cases we refer to Reference [23].

6.1. *Computational domain, boundary conditions and numerical grids*

The computational domain and the boundary conditions are shown in Figure 4. All computations were carried out for the Reynolds number $Re_{\text{L}} = \text{L}^* = U_\infty \text{L}/\nu = 1.6 \times 10^5$, based on the inflow velocity (U_∞) and the length of the plate located in the computational domain (L). This Reynolds number ensures that the boundary-layer flow is fully developed at the outlet. Hence the Blasius solution can be applied as boundary condition at a part of the outlet. On the other hand, this value is still much smaller than the lower limit of the critical Reynolds number of transition, namely $Re_{\text{crit}} = 3.2 \times 10^5$ according to Schlichting [31]. In order to reduce the influence of the boundary condition on the numerical solution in the region of interest, a large domain height, $\text{B}^* = 2 \times 10^4$, was chosen. This corresponds to 100 times the non-dimensional boundary-layer thickness at $x^* = \text{L}^*$, namely $\delta^*_{\text{L}} = 5/Re^{1/2}_{\text{L}}$. For the same reason, the computational domain was extended to $\text{L}^*_f = 0.2\text{L}^*$ upstream from the leading edge.

The flow was assumed to be undisturbed at the inlet and at that part of the upper boundary upstream of the flat plate ($U^* = 1$ and $V^* = 0$). At the lateral boundary and at the outflow plane a fully developed flow ($\partial\phi/\partial y = 0$, $\phi = U^*, V^*$ and P^*) was assumed except in the near-wall region which was approximated by the Blasius solution as mentioned above. For the boundary in front of the leading edge, symmetry conditions are applied, namely $\partial U^*/\partial y^* = 0$ and $V^* = 0$. At the wall no-slip boundary conditions ($U^* = 0$ and $V^* = 0$) are used. Finally, the local asymptotic solutions (16) and (17) were assigned at the *Stokes inlet*.

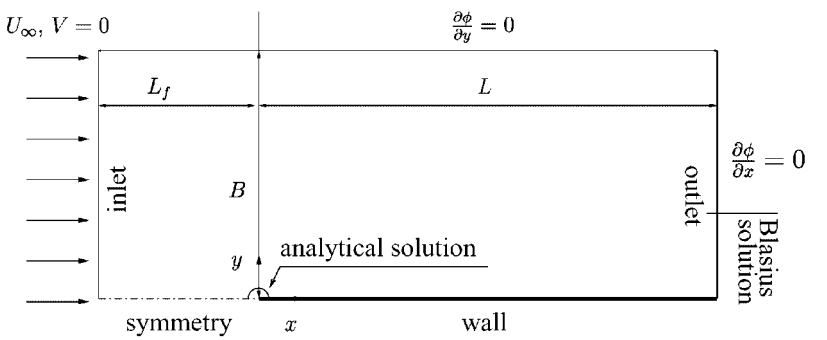

Figure 4. Sketch of the computational domain and boundary conditions.

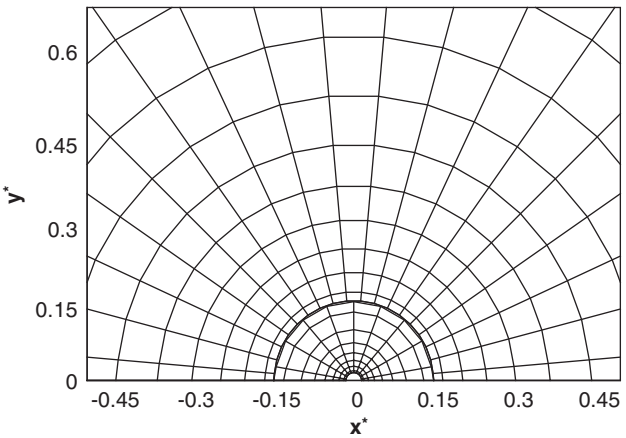

Figure 5. Numerical grid of the matching region, shown for CV centres at the first (coarsest) grid level.

The numerical grids consist of five multi-grid levels and contain 2240 CVs on the first (coarsest) grid level leading to about 5.8×10^5 CVs on the finest level. Local grid refinement was applied to obtain an extremely fine grid resolution in the region of interest. A zoomed view of the numerical grid around the leading edge is depicted in Figure 5. The *Stokes inlet* was set at $r^* = 0.015$. The CVs used for the matching of the numerical and analytical solutions were located in the block closest to the leading edge, which has a size of $0.015 \leqslant r^* \leqslant 0.15$. In this block, 10 equidistant grid points were applied at the Stokes inlet (in the i direction, i.e. tangential direction) and eight grid points, whose intervals were expanded by a power of 1.3, were used in the j direction (radial direction). The minimum grid size is $\Delta r^* = 7.7 \times 10^{-3}$ at the first grid level and $\Delta r^* = 4 \times 10^{-4}$ at the fifth grid level. In comparison, much coarser grid resolutions were applied to the flow region far away from the leading edge and outside the boundary layer in order to achieve efficient calculations for the flow of interest. For this reason, convergence can only be obtained at the finest grid level for calculations using the CDS scheme.

6.2. *Influence of the matching location and matching points*

Adopting the *least-square* matching strategy one needs much more matching CVs than the number of coefficients of the local solution. Hence, it is worth investigating how many matching CVs are necessary for a reliable *least-square* matching. The location of the matching CVs is also of importance for the accuracy of the numerical results as indicated by the error analysis in Section 5. In order to obtain reliable matching computations and to be confident about the numerical accuracy, a number of numerical experiments using varying numbers (n) and locations of matching CVs were carried out. The case where the matching CVs are located along a grid line is denoted *line matching* while the case when the matching CVs are distributed in a zone is called *region matching*. In all test cases, the distance of the matching CVs from the leading edge are within a range $0.015 < r_0^* < 0.1$. Matching grid lines along both i and j directions and matching zones of different sizes were tested. Here, we present the results from two representative cases, whose matching locations are sketched in Figure 6.

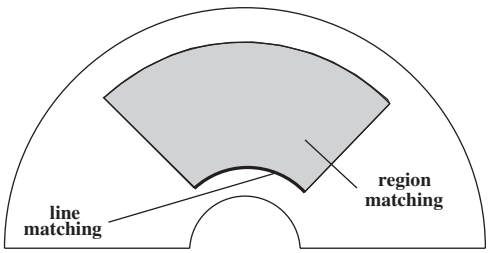

Figure 6. Sketch of two characteristic matching locations for line matching ($r_0^* = 0.03$, $n = 146$ CVs on fifth grid level) and region matching ($0.03 \leqslant r_0^* \leqslant 0.09$, $n = 1073$ CVs on fifth grid level).

Table I. Comparisons of the coefficients of the local solution determined by the line-matching and region-matching strategy; grid convergence rate estimated by p_k; Richardson extrapolation applied to drop the discretization error in A_i; computations based on a local asymptotic solution containing the first three expansion terms ($m = 3$) in Equations (16)–(18).

k	p_0	A_1	p_k	A_2	p_k	A_3	p_k
Line matching							
1	−0.17695370	0.20600677		0.11401301		0.75431480	
2	0.11940396	0.19314444		2.81705849E-02		0.14676585	
3	0.13949590	0.19001189	2.04	5.53510530E-03	1.92	1.01310592E-02	2.15
4	0.13704437	0.18982919	4.10	3.87060966E-03	3.77	4.07408741E-03	4.50
5	0.13473557	0.18979424	2.39	3.42530042E-03	1.90	2.85725575E-03	2.32
extrapolation		0.18979		3.2769E-03		2.5531E-03	
Region matching							
1	0.12631758	0.19180704		3.08230814E-02		5.21052431E-02	
2	0.14617762	0.19011551		7.14135036E-03		1.18953485E-02	
3	0.14135558	0.18987562	2.82	4.75805710E-03	3.31	6.97434251E-03	3.03
4	0.13736588	0.18982849	2.35	4.08442989E-03	1.82	5.42922803E-03	1.67
5	0.13484245	0.18981582	1.90	3.82425261E-03	1.37	4.83244282E-03	1.37
extrapolation		0.18981		3.6619E-03		4.4604E-03	

In both tests, a local solution containing three expansion terms ($m = 3$) was applied and U^* was chosen as the matching variable. For a complete set of results refer to Reference [23].

6.2.1. Results for coefficients. The numerical results of both test cases for the coefficients of the local solutions (16)–(18) (p_0 and A_i) are displayed in Table I. The grid convergence rates p_k of the coefficients A_i were also analysed based on the numerical results at successive multi-grid levels k (see Reference [32]). Based on the grid convergence rate p_k obtained, Richardson extrapolation was applied for the coefficients A_i in order to drop the discretization error. The results obtained for p_k and the extrapolated A_i are also presented.

The coefficients of the leading expansion A_1, calculated from different test cases are very close to each other, with a maximum difference of about 4×10^{-4} absolute or 0.2% relative. In addition, it can be concluded that A_1 increases with decreasing distance (r_0^*) of the matching CVs from the leading edge. The deviations in A_2 begin from the second dec-

imal number. Nevertheless, since A_2 is two orders of magnitude smaller than A_1 and since $r_0^* < 0.1$ in all cases, the influence of these deviations on the local solution is expected to be one order of magnitude smaller than the error caused by the deviations in A_1. It is noted that the results for A_3 obtained by the *line matching* strategy differ significantly from those obtained with *region matching*. The results indicate that A_3 is of the order $O(10^{-3})$, but a closer evaluation is impossible. A comparison of the third and the first expansion terms gives $A_3 r_0^{*2}/A_1 r_0^{*0.5} = (A_3/A_1) r_0^{*1.5} \sim O(10^{-3.5})$ (refer to Equation (16)), which is already smaller than the relative deviations of A_1. That explains the reason.

With reference to Equation (30), the discretization accuracy for the Stokes flow is of the order $O(r_0^{*-1.5} h^2)$. Hence fixing r_0^*, the coefficients A_i are expected to have a second-order grid convergence rate (p_k) as supported by the numerical results of the line-matching strategy. The grid convergence rate was found to decrease with increasing r_0^*. This is not due to the increasing influence of the convective term (first-order UDS discretization) at the matching locations of this case in view of the error analysis (Equations (44) and (45)). The real cause might be that the larger expansion error $[O(r_0^{*2.5})]$ dominates over the discretization error $[O(r_0^{*-1.5} h^2)]$ in this case, as indicated by the quantitative error estimations [23]. As a result, the discretization accuracy is partially destroyed.

It is not possible to perform grid-convergence analysis for p_0, since the change of the results at varying grid levels is not always monotonic. This might be due to the variation of the pressure reference point at different grid levels. Nevertheless, the pressure gradient rather than the pressure itself is relevant for the velocity field. Hence, a change of the pressure reference point at different grid levels is not a critical issue for the numerical solution. In addition, p_0 is passive and does not have an influence on the coefficients A_i since a matching procedure based on U^* was adopted (refer to Section 3).

It was observed that a matching asymptotic calculation using the *line matching* sometimes failed to converge or the coefficients converged to wrong values. In contrast, the *region matching* was found to be robust. In practice, it might occur that some terms of the local solution can happen to be zero along a matching grid line or the solution is disturbed at a matching location. In these cases a computation adopting the *exact matching* strategy or the *least-square* matching strategy but based on a *line matching* can fail. For this reason we recommend the *least-square region-matching* strategy.

6.2.2. Matching residuals. The matching residuals (46) of the above test cases, which were evaluated over the matching CVs of the *region-matching* case, are presented in Table II. It is found that δ_{U^*} and δ_{V^*} decrease monotonically with decreasing grid size (or increasing grid level k) and that at the fifth grid level δ_{V^*} is about $10^{-3}\delta_{U^*}$ in all computations. Moreover, δ_{U^*} and δ_{V^*} are much higher in the case of *region matching* than those of *line matching*.

The grid size varies from 4.0×10^{-4} to 1.7×10^{-3} in the maximum range ($0.015 < r_0{}^* < 0.1$) of the matching locations of all test cases and the control region for the residual evaluation. Based on this information, the matching residual is expected to be about $O(10^{-8}) - O(10^{-10})$ for δ_{U^*,V^*} and about $O(10^{-4}) - O(10^{-6})$ for δ_{P^*} according to the error estimation (47) and (48). Hence the present matching residuals for all variables are reasonably low.

It is noted that δ_{P^*} remains of the same order from the fourth to the fifth grid level. This indicates that the effect of the grid size is negligible and thus δ_{P^*} is dominated by the approximate equation error $[O(r_0^{*2})]$ rather than by the discretization error $[O(r_0^{*-5} h^4)]$. Such behavior is also observed for δ_{U^*} for the cases adopting the *region matching* and the

Table II. Comparisons of the residual of the global solution and the matching residuals (46) calculated based on the line- and region-matching strategy, where k represents the grid level and n denotes the number of the matching points. Computations were based on a local asymptotic solution containing the first three expansion terms ($m = 3$) of Equations (16)–(18).

k	n	ε_{num}	δ_U	δ_V	δ_P
Line matching					
1	12	4.65362727E-08	9.43298536E-07	7.86082114E-08	5.75094931E-02
2	22	4.39171718E-07	9.21452707E-07	3.07150902E-08	2.79299940E-03
3	38	9.40864449E-08	2.53334315E-09	3.16667893E-11	1.03779353E-07
4	74	9.47255890E-08	1.09789159E-10	3.85225118E-13	2.46695226E-06
5	146	9.85809260E-08	4.85673107E-12	4.52631041E-15	3.37869764E-06
Region matching					
1	9	9.93673865E-08	1.75927331E-07	1.46606109E-08	6.34994887E-04
2	30	4.39171732E-07	1.73848021E-06	5.79493404E-08	3.90252379E-06
3	80	9.93241293E-08	2.65106532E-07	3.31383165E-09	1.28747030E-06
4	285	9.63074901E-08	1.38359968E-07	4.85473573E-10	9.63960743E-07
5	1073	9.86387180E-08	1.06415672E-07	9.91758362E-11	9.59728956E-07

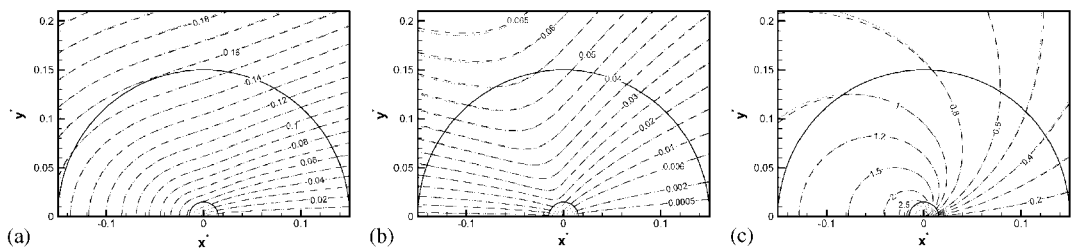

Figure 7. Comparison of the numerical solution (N-S equations, *dashed*) and the analytical solution (Stokes equations, *dotted*) for the flow close to the leading edge obtained by region matching; displayed for the isolines of: (a) U^*; (b) V^*; and (c) P^*.

line matching at the location $r_0^* \approx 0.09$. Consequently, the results from the above numerical experiments support the error estimation (47) and (48). In addition, it is observed that δ_{V^*} is smaller than δ_{U^*}. Nevertheless, the regular relation between both residuals ($\delta_{V^*} \approx 10^{-3}\delta_{U^*}$) might be related to some specific feature of the flow in the present problem.

In contrast to the significant effect of the matching location, the number of matching CVs does not show an important influence on the matching asymptotic calculation. The minimum number in all test cases (partially not shown here) was $n = 74$ at the fifth grid level.

6.2.3. Range of validity of the local solution. It is of interest to examine the range of validity of the Stokes approximation. For this purpose, the numerical solution (ϕ_h, N-S equations) and the analytical solution (ϕ_{anal}, Stokes equations) based on the coefficients determined by the matching procedure in the flow field close to the leading edge were compared. As an example, the isolines of the velocity components and pressure distribution based on both solutions using region matching are depicted in Figure 7 for the region of interest. The results indicate that

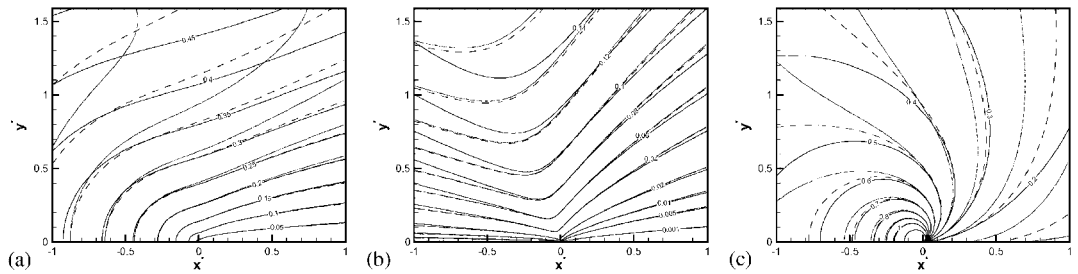

Figure 8. Examination of the range of validity of the Stokes solutions based on the coefficients obtained by *line matching* (*dashed*) and *region matching* (*dotted*) by comparison with the numerical solution of the combined analytical–numerical method using region matching (N-S equations, *solid*); displayed for the isolines of: (a) U^*; (b) V^*; and (c) P^*.

both solutions agree very well with each other at least up to $r_0^* \leqslant 0.15$, which is already beyond the range of the matching region of all cases. Consequently, the present computations are reliable.

Furthermore, it is of interest to find out which matching strategy provides more accurate results. The answer becomes clear from a comparison of the range of validity of the analytical solutions based on the coefficients obtained by both strategies. For that purpose, Figure 8 displays isolines for the velocity and pressure distributions obtained by the analytical solutions of the *line-matching* case and the *region-matching* case together with the numerical solution of the combined analytical–numerical method using region matching. Consequently, the Stokes solution using the coefficients of the *line-matching* case has a larger range of agreement with the numerical solution than that based on the coefficients of the *region-matching* case. This is consistent with the matching residuals discussed above, and is due to the smaller distance of the matching CVs from the leading edge in the former case.

6.3. *Influence of the expansion order*

Numerical experiments were carried out by using a local solution including varying number of terms ($m = 1, 2, 3, 4$ and 6) in order to investigate the effect of the local expansion order. Again U^* was chosen as the matching variable and the investigations were done both for *line* and *region* matching. For reference, Figure 9 displays the isolines of the velocity components and the pressure predicted by line matching with expansion terms of $m = 1, 3$ and 6. It is again noted that the coefficients of the leading expansion A_1 are very close to each other in all computations, with the maximum deviation being less than 0.1% for *line matching* and 0.04% for *region matching*. The deviations in the coefficients of the higher-order terms are larger. Nevertheless, the errors due to that are within the magnitude resulting from the deviations of the leading expansion, owing to the small magnitude of the higher-order terms. Owing to this fact, although converged results can be obtained for the coefficients of higher-order expansions, they are not accurate. On the other hand, the numerical results show that the higher-order terms are useful for reducing the matching residuals and for improving the grid convergence rate of the lower-order coefficients.

Additionally, it is noted that δ_{P^*} is dominated by ${r_0}^*$ in all computations. This is also true for the results for δ_{U^*} in the *line-matching* case if lower-order expansions ($m = 1$ and 2) were

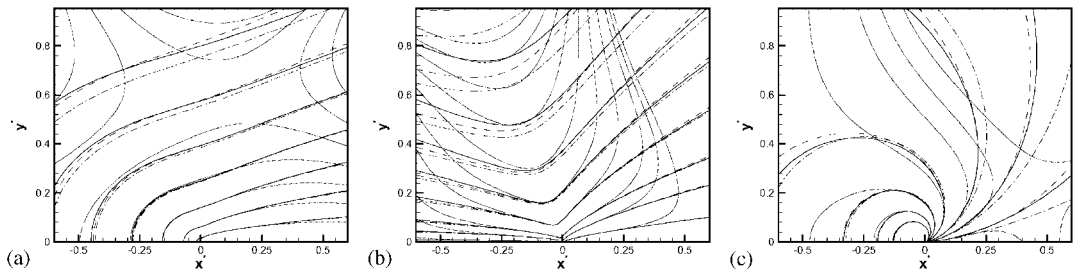

Figure 9. Numerical results for the flow close to the leading edge using line matching. Comparison of the effect of the expansion order: Stokes solutions with $m=1$ (*dash–dotted*), $m=3$ (*dashed*), $m=6$ (*dotted*) and numerical (N-S) solution (*solid*): (a) U^*; (b) V^*; and (c) P^*.

applied and in the *region-matching* case for all orders of expansions (up to $m=6$). A detailed analysis [23] confirm that the reason for this behavior is due to the dominant expansion errors in these cases using the present grid (h) and matching locations (r_0^*). As a consequence, it is useful to improve the numerical accuracy by moving the matching locations closer to the singular point. The analysis also shows that the magnitudes of the matching residuals at the fifth grid level are reasonable with reference to the error estimations (44) and (45).

It is worth mentioning the test cases with $m=4$ and 6. The convergence of the *line-matching* case is found to be much slower than that of *region matching*. Furthermore, it is found that in the case of using the full expansion given by Equations (16)–(18), i.e. $m=6$, ε_{A_4} remains larger than ε_{A_5} and ε_{A_6} in the process of the iterative solution at the fifth grid level. This slows down the convergence of the coefficients of the higher-order terms. These results confirm again that the *region-matching* strategy is more robust than the *line-matching* strategy. Moreover, it is worth noting that the fourth expansion term has a higher order ($\lambda_4=2.5$) than that of the approximate equation error $d\phi_{\mathrm{eq}}$ ($2\lambda_1+1=2$). As pointed out in Section 5, the coefficient of this term or even higher-order terms might be inaccurate.

6.4. *Influence of matching variable*

As mentioned in Section 3, a matching asymptotic computation can be based on each of the dependent variables, U^*, V^* or P^*, or any combination of them, considering that the local solution (16)–(18) involves the same coefficients (A_{λ_i}). Nevertheless, the numerical experiments indicate that the matching variable has an important influence on the accuracy and properties of convergence. For example, according to the error estimations (44) and (45), the numerical accuracy of P^* is expected to be one order of magnitude lower with respect to $r_0{}^*$ than that of the velocity components. Thus the disadvantage of choosing P^* as the matching variable is clear. In addition to the lower accuracy, a matching calculation based on P^* failed to converge if the multi-grid method was applied. This is related to the large pressure adjustments occurring during shifts of the grid levels. As pointed out in Section 3, p_0 is not passive in this case, and a pressure change will result in large disturbances in the velocity assigned at the Stokes inlet and thus lead to divergence of the computation.

Differences were also observed between computations based on matching for U^* and V^*. To demonstrate this effect, numerical experiments based on both matching variables and using

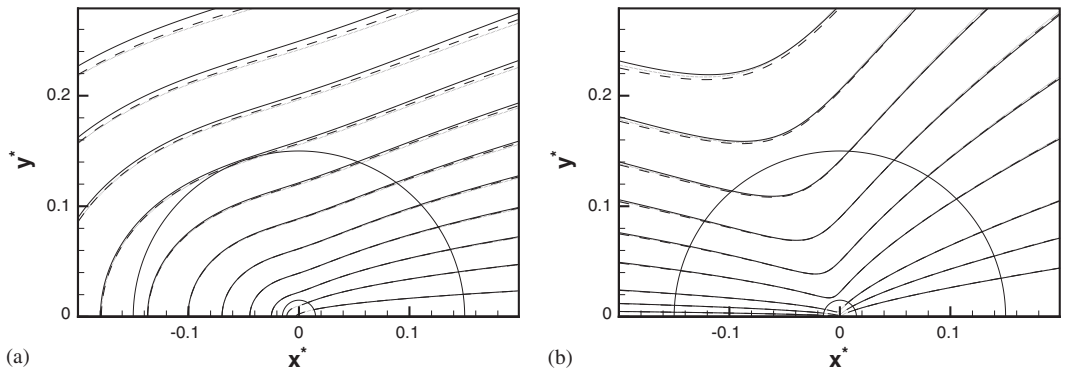

Figure 10. Comparison of the Stokes solution based on the coefficients obtained from U^* matching (*dashed*) and from V^* matching (*dotted*) with the numerical solution of the Navier–Stokes equations (*solid*) for the flow close to the leading edge; displayed for the isolines of U^* (left) and V^* (right) for the line-matching case ($r_0^* \approx 0.03$) with $m = 2$.

both line and region matching were carried out. The results (not displayed here, refer to Reference [23]) show that the grid convergence rate of the coefficients from computations based on V^* as the matching variable are less regular than those obtained by matching for U^*. The results for the matching residuals also indicate that the performance of V^* matching was generally worse than that of U^* matching. Furthermore, slower convergence or even divergence was more often observed in the *line-matching* case when V^* was chosen as the matching variable. Therefore, it can be concluded that the matching variable has an important influence on the matching asymptotic computation. However, there is no reason to conclude that it is generally of advantage to choose U^* as the matching variable. The better performance in the case of matching for U^* observed in the present study should be related to the special flow features of the present problem. In addition, the Stokes solution with the coefficients computed based on both matching variables agree well with the numerical solution (N-S) at least in the range $r_0^* \leqslant 0.1$, which is demonstrated by the isolines of U^* and V^* depicted in Figure 10.

6.5. *Influence of the differencing scheme*

Finally, it is also interesting to make an examination on the influence of the differencing scheme. For this purpose, several numerical experiments were carried out using the second-order CDS discretization for the convective terms. This scheme was only applied at the fifth grid level considering the convergence difficulty at coarser grid levels due to the large grid sizes in the flow region out of interest. A comparison of the numerical results for the corresponding coefficients with those obtained by applying the UDS discretization (convective terms) was carried out. In both cases the diffusion terms were discretized by the second-order accurate CDS scheme. It is found that the difference in the results obtained using the two different schemes for the convective terms is negligible. This is due to the fact that the convective terms of the N–S equations can be neglected near the leading edge where Equation (11) is satisfied. Consequently, the application of modern high-order formulations such as compact schemes will lead to the same conclusion. However, the effect of the differencing scheme on

the pressure and diffusion terms is not expected to be negligible, as indicated by the error analysis described in Section 5.

6.6. Numerical solution with local grid refinement

For comparison, purely numerical simulations without using the matched asymptotic algorithm were also carried out. In this case, the computational domain was decomposed into 49 rectangular blocks. The grids were highly refined for those blocks located in the proximity of the leading edge and in the boundary layer of the plate, which results in a finest grid resolution $\Delta x^* = 0.001$ at the finest (fifth) grid level. In order to demonstrate the grid convergence effect of the local grid refinement, comparisons of the solutions at the third and fifth grid levels were done. The results show that the numerical solutions of the velocity components (U^* and V^*) converge with finer numerical grids, except for some disturbances at the direct neighbour CVs of the leading edge. In contrast, the solution of the pressure diverges and the solution cannot be improved by means of local grid refinement. Therefore, the above results confirm the results of the error analysis, namely Equations (44) and (45).

7. PHYSICAL ANALYSIS AND DISCUSSION

Finally, the physical features of the incompressible laminar flow past a semi-infinite flat plate such as the drag coefficients, the development of the boundary layer over the plate, and the flow field around the leading edge, will be discussed. In order to draw reliable conclusions from the study, the discussion is based on the numerical results obtained by using the second-order accurate CDS discretization for the convection term.

7.1. Results for the flow field

The isolines of the velocity components and the vorticity of the flow in the range of distance $r_0^* \leqslant 10$ from the leading edge are demonstrated in Figure 11(a)–11(c). In order to have a clearer picture of the flow around the leading edge, the results of the stream function are also presented in Figure 11(d). Owing to the no-slip effect of the wall, it is observed in this figure that the flow displaces away from the wall in the y direction. Nevertheless, the displacement already starts upstream of the leading edge rather than at the leading edge itself as assumed in the Blasius solution. This flow displacement results in a small flow region close to the leading edge where V^* reaches the maximum value of the total flow field [Figure 11(b)].

The Stokes flow in the direct neighbourhood of the leading edge is dominated by diffusion (governed by elliptic equations). For this reason, it is observed that the magnitudes of $\partial U^*/\partial x^*$ and $\partial U^*/\partial y^*$ are close to each other upstream of the leading edge. Figure 11 indicates that the diffusion effect is still important in the flow region $r_0^* \leqslant 10$. Despite the rapid decay of ω^* in the upstream direction, both $\partial U^*/\partial x^*$ and V^* are still of considerable significance in this region. Furthermore, it can be noted that $\partial \omega^*/\partial y^* < 0$ at the wall ($x^* \geqslant 0, y^* = 0$). This result is similar to that of Botta and Dijkstra [8], which was also obtained based on the Navier–Stokes equations. This non-zero gradient, $\partial \omega^*/\partial y^*|_{x^* \geqslant 0, y^* = 0}$, physically corresponds to a vorticity production at the wall. In contrast, it is assumed that $\partial \omega^*/\partial y^*$ vanishes at the wall in the Blasius solution. As a result, the entire vorticity production has to be sought at the leading edge in the boundary layer theory. The above results are sufficient to show that

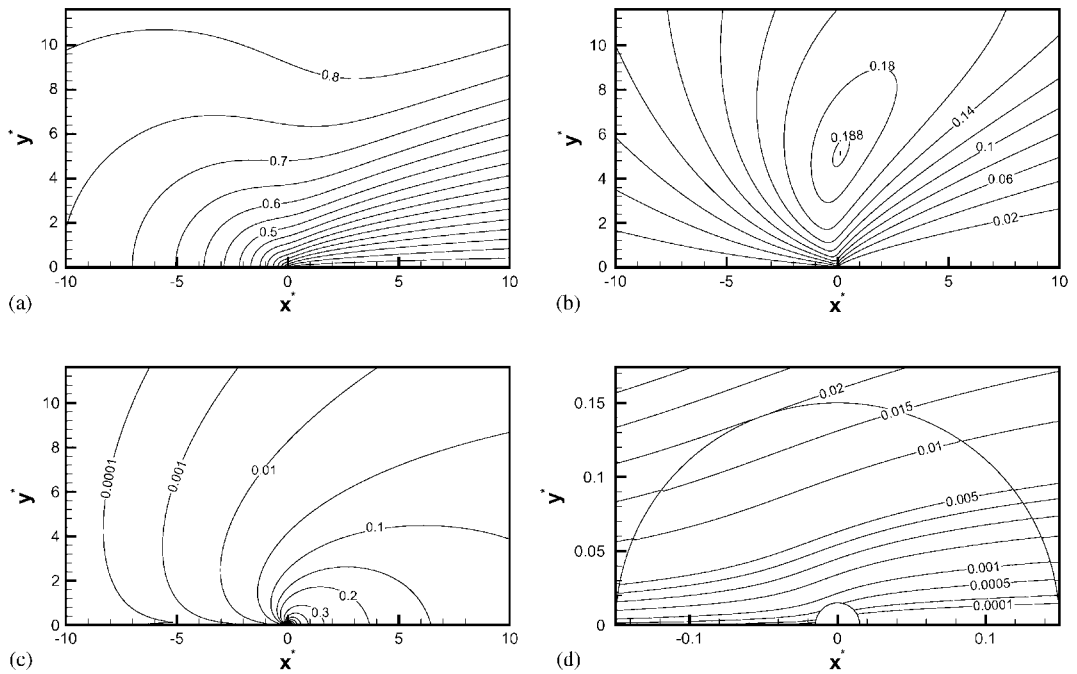

Figure 11. Laminar incompressible flow close to the leading edge of a semi-infinite plate; isolines of U^* (a), V^* (b) and ω^* (c) for $-10 \leqslant r_0^* \leqslant 10$; stream function for $-0.125 \leqslant r_0^* \leqslant 0.125$ (d).

boundary layer theories of varying orders (parabolic assumption) do not apply to the flow region close to the leading edge. From this point of view, some classical analytical work in the literature, which represent the efforts to take the leading-edge effect into account by developing higher-order boundary layer theories [33] or to solve the flow near the leading edge by matching the Stokes solution to the Blasius solution [1], are not physically justified. The predicted flow field shows that the influence of the plate (diffusion effect) extends far away from the Blasius boundary layer both in the y direction and in the negative x direction.

7.2. *Development of the boundary layer flow*

The velocity profiles displayed in Figure 12 provide a picture for the development of the boundary layer flow over the semi-infinite flat plate. The results are presented for the similarity variables following the Blasius solution, namely U^* $(= U/U_\infty)$ vs η and $V^* Re_x^{1/2}$ vs η, respectively. Here η is defined as $\eta = y\sqrt{U_\infty/(vx)} = y^*/\sqrt{x^*}$. The results of the Blasius solution are also plotted for comparison. Significant deviations exist between the present velocity profiles and those according to the similarity solution of Blasius for fully developed boundary layer flow, especially at $x^* = Re_x \leqslant 100$. The latter is obtained from the simplified Navier–Stokes equations based on perturbations for $Re_x \to \infty$. At $Re_x \geqslant 1000$, the Blasius solution becomes a good approximation, as evident in Figure 12.

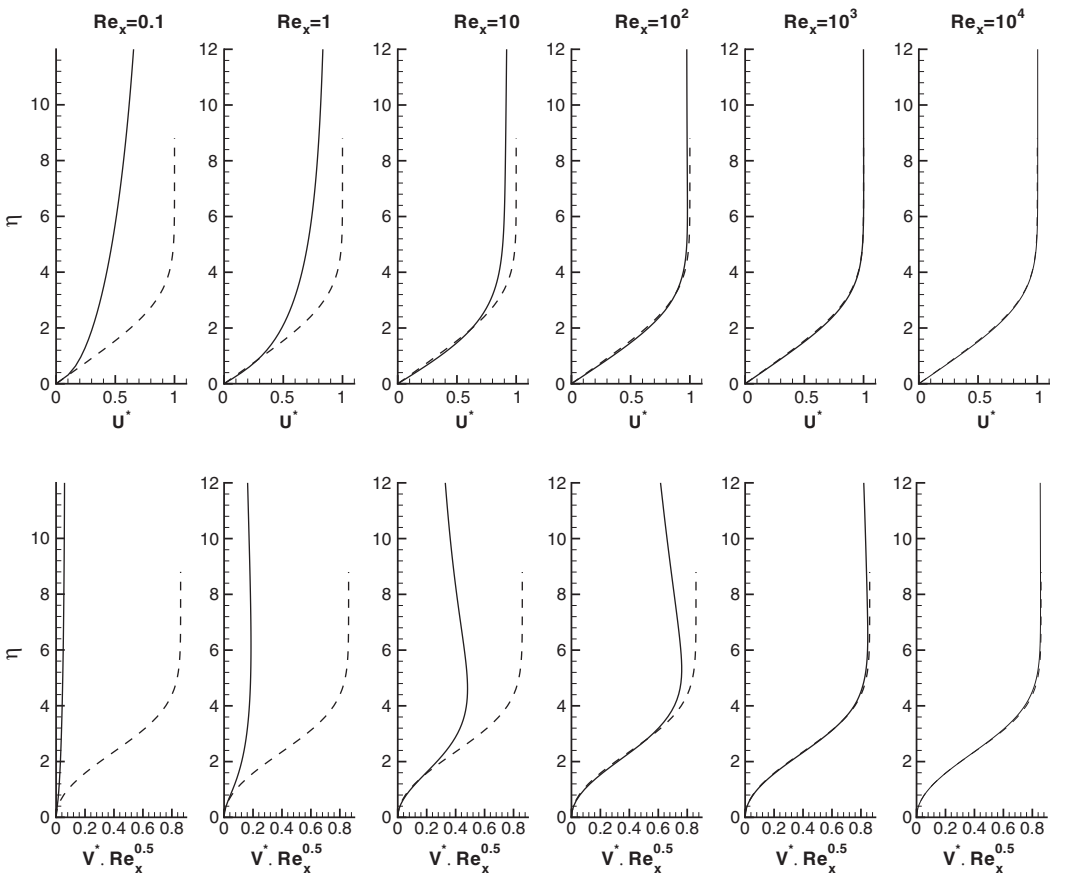

Figure 12. Development of the velocity profiles U^* vs η and $V^*Re_x^{1/2}$ vs η of the incompressible laminar flow over a semi-infinite flat plate.

7.3. Local skin friction

7.3.1. Results near the leading edge. At $Re_x \to 0$, the local skin friction c_f at a flat plate can be well estimated from the local analysis of the Stokes flow given by Equation (20). As an example, the results for the line-matching case with a varying number of expansion terms are displayed in Figure 13. As expected, all results based on the Stokes approximation agree very well with each other and with the numerical solution of the Navier–Stokes equations at $Re_x \leqslant 0.1$. This is due to the fact that the leading-order term is dominant in Equation (20). For example, the ratio of the second to the first term of Equation (20) is equal to $3A_2/A_1Re_x$, which is expected to be less than 0.7% at $Re_x \leqslant 0.1$ according to the results of the coefficients. The higher-order terms decay even more rapidly when $Re_x \to 0$, and hence are trivial.

It is interesting to note in Figure 13 that the skin friction resulting from the leading expansion of the Stokes equations ($m = 1$) agrees fairly well with the numerical results of the Navier–Stokes equations in the entire range up to $Re_x = 10$. This is due to the dominant

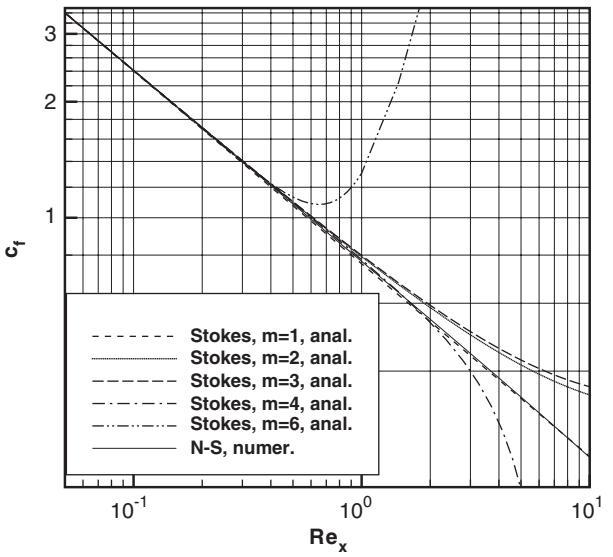

Figure 13. Comparison of the Stokes flow approximation (20) of varying expansion orders and the numerical results of the Navier–Stokes equations for the local skin friction c_f around the leading edge of a semi-infinite flat plate displayed for the line-matching case.

viscous effect close to the wall surface (small y^*). No significant extension is observed for the validity range of the Stokes approximation for the skin friction result (20) in the case when higher-order terms are involved. However, their agreement with the numerical results of the full Navier–Stokes equations at $Re_x \to 0$ is improved, as discussed in Section 6.3.

It is worth pointing out that Equation (20) differs from the local asymptotic solution by Carrier and Lin [1] in the higher-order terms, e.g. the third term in their relation which is $O(Re_x^1)$ compared with $O(Re_x^{3/2})$ in Equation (20). This is a result of the different asymptotic solutions used in the present study and by Carrier and Lin [1]. Nevertheless, both solutions are acceptable considering that the higher-order terms are negligible at $Re_x \to 0$. Therefore, it is already sufficiently accurate to consider the first two terms of Equation (20) for c_f at the leading edge, namely

$$c_f = ARe_x{}^{-1/2} + BRe_x{}^{1/2} + \cdots \tag{49}$$

where $A = \lim_{Re_x \to 0}(c_f Re_x^{1/2})$ is dominant according to the quantitative evaluation discussed above.

A comparison of the present results (line matching with $2 \leqslant m \leqslant 4$) for A and B with those available in the literature is summarized in Table III. It is noted that the influence of the expansion order m on the leading coefficient A is small. The present results for this coefficient agree very well with the value calculated by Botta and Dijkstra [8], with a difference being less than 0.6%. In comparison, the result from the Blasius solution is about 12.5% smaller than the present values.

In contrast to A, the results obtained for B ($= 12A_2$) vary in a wider range with varying expansion orders m. Nevertheless, the effect of this variation on the skin friction is not of

Table III. Comparison of the skin friction coefficients at the leading edge with the literature; a dash means that this value was not given by the authors.

Author	$A = \lim_{Re_x \to 0} (c_f Re_x^{1/2})$	B
Blasius solution	0.664	0
Lewis and Carrier [34]	1.128	—
Dean [35]	0.796	—
Davies [36]	0.779	—
Yoshizawa [37]	0.748	0.044
Botta and Dijkstra [8]	0.75475	0.041
Present result ($2 \leqslant m \leqslant 4$)	0.75888–0.75916	0.03382–0.03932

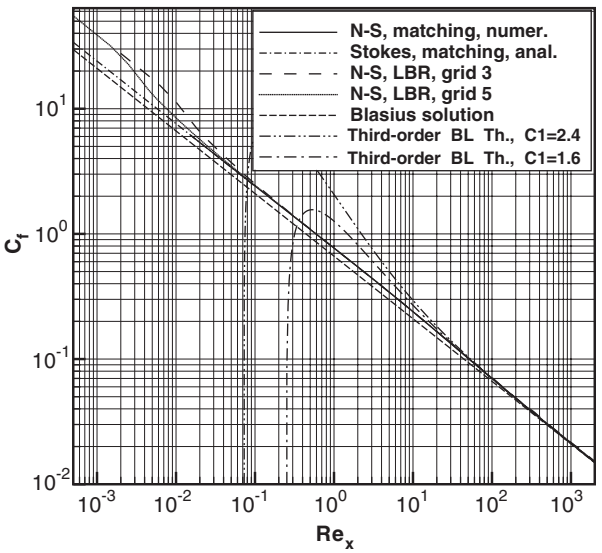

Figure 14. Comparison of the present results for the local skin friction c_f obtained from the matching asymptotic calculations with those obtained by local block refinement and the classical results from different boundary layer theories.

significance, considering that the total contribution of the second term is minor at $Re_x \leqslant 0.1$, according to the quantitative evaluation discussed above.

7.3.2. Comparison with boundary layer theories. A comparison of the present results with the Blasius solution and the result from the third-order boundary layer approximation due to Goldstein [38] and Imai [33] is demonstrated in Figure 14. The latter one yields the following results for the local skin friction coefficient:

$$c_f \approx 0.664 Re_x^{-1/2} + 0.551 \log(Re_x) Re_x^{-3/2} + (C_1 - 1) Re_x^{-3/2} + \cdots \tag{50}$$

The results (on the third and fifth grid levels) obtained by the local block refinement technique (LBR) instead of using the matching asymptotic algorithm are also plotted for reference.

Compared with the matching asymptotic computation, the LBR results are disturbed in the range $Re_x \leqslant 0.1$, even when a very fine local grid resolution of $Re_{\Delta x} = \Delta x^* = 10^{-3}$ at the fifth grid level is used. This is due to the pollution effect of the leading-edge singularity. Nevertheless, the difference between the results obtained from both calculations is negligible for $Re_x \geqslant 1$. Figure 14 shows that the Blasius solution underestimates the skin friction in the range $Re_x < 1000$. The difference between the Blasius solution and the present results decreases with increasing Re_x to a level within 1% at $Re_x \geqslant 1000$. The skin friction resulting from the third-order boundary layer approximation (Equation (50)) contains an undetermined coefficient C_1. Its value was estimated to be $2.2 < C_1 < 2.5$ and $C_1 \approx 1.6$ by the numerical solution of Botta and Dijkstra [8] and Yoshizawa [37], respectively. The results plotted in Figure 14 are based on $C_1 = 1.6$ and 2.4. Comparison with the present results (N-S solution) indicates that the local skin friction predicted by the third-order boundary layer approximation is valid for Reynolds numbers down to $Re_x = 100$, with a deviation less than 1%. Compared with the validity range of the Blasius solution, this improvement due to the third-order boundary layer approximation is significant.

Theoretically, C_1 can also be estimated based on the present results for c_f, leading to:

$$C_1 = c_f Re_x^{3/2} - 0.664 Re_x - 0.551 \log(Re_x) + 1 \tag{51}$$

Nevertheless, one has to recall that the numerical error in c_f will be enlarged by a factor $Re_x^{3/2}$. Moreover, Equation (50) is only valid at $Re_x \geqslant 100$, as shown in Figure 14. As a result, a closer estimation is not available from the above method. For this reason, no further effort to calculate C_1 was made in the present study.

8. CONCLUSIONS

Angular singularities require special treatment in flow predictions, since a finite discretization scheme looses local and global accuracy in the vicinity of angular points (sharp edges or corners). Using a primitive variable formulation of the Navier–Stokes equations, this problem is especially severe for the pressure, whose numerical solution diverges in the proximity of angular singularities. In order to improve the accuracy of numerical predictions, a generally applicable combined analytical–numerical treatment for angular singularities has been developed in the present work. The methodology is based on a computational matching asymptotic algorithm taking advantage of the analytical (asymptotic) solution, which can be obtained for the local Stokes flow around an angular point. This procedure avoids the numerical solution in this critical region. As a result, the finite discretization is restricted to a regular domain without perturbations and pollutions induced by singularities.

The local asymptotic solution applied involves unknown coefficients. They are determined by matching this solution to the numerical solution in the flow region where the Stokes approximation holds. A formal error analysis has been derived for this combined algorithm, which serves as a useful guide for designing appropriate numerical grids for the practical application. In order to make the entire algorithm robust and efficient, numerical experiments were carried out to investigate the effects of different, more or less important influencing factors on the numerical results, such as the matching location, the matching variable, the order of asymptotic expansions and the differencing scheme (UDS or CDS), etc. Furthermore,

the convergence properties of the matching asymptotic computation were determined. The numerical experiments show the desirable properties of the present algorithm, i.e. accuracy, robustness and efficiency. Moreover, the results from the numerical experiments are in support of the error estimations derived.

Based on this algorithm, accurate numerical results have been obtained for the flow near the leading edge and for the coefficients of the local asymptotic solution. Physical analyses were carried out for the results predicted and the validity of the boundary layer theory of varying orders was examined. Based on these investigations, the following conclusions can be drawn:

- Using a uniform grid size h, the numerical solution in the direct neighbourhood of an angular point has a maximum accuracy of the order $O(h^{\lambda_1})$ for the velocity field and $O(h^{\lambda_1-1})$ for the pressure, where λ_1 is the smallest positive eigenvalue depending on the angle of the corner, if a discretization scheme of second-order accuracy is directly applied. This corresponds to an accuracy of the order $O(h^{1/2})$ for the velocity components near the leading edge of a semi-infinite plate whereas the pressure diverges at an order of $h^{-1/2}$ in the direct vicinity of the edge. This demonstrates that even applying modern numerical techniques such as adaptive grids or local block refinement as in the present work is not an appropriate manner to tackle singularities.
- With the combined analytical–numerical algorithm, the accuracy of the numerical solution around an angular point can be improved to the order $O(r_0^{*\lambda_1-2}h^2,\ r_0^{*2\lambda_1+1},\ r_0^{*\lambda_{m+1}})$ for the velocity components and $O(r_0^{*\lambda_1-3}h^2, r_0^{*2\lambda_1}, r_0^{*\lambda_{m+1}-1})$ for the pressure, where r_0^* is the radial distance from the matching location to the angular singularity.
- According to the present results for the velocity profile and the local skin friction, the Blasius boundary layer solution can be considered as a good approximation for the incompressible laminar flow over a semi-infinite flat plate at $Re_x \geqslant 1000$. In comparison, the range of validity of the local skin friction is extended to $Re_x \geqslant 100$ using the third-order boundary layer theory for the semi-infinite plate.
- The present results show that the flow close to the leading edge is dominated by diffusion (elliptic equation). Hence boundary layer theories of any order, which are based on the parabolic assumption, ceases to describe the physical effects reasonably and thus cannot be applied. Compared with the present results, the local skin coefficient according to the Blasius solution is about 12.5% smaller at the leading edge ($Re_x \to 0$).

In conclusion, the combined analytical–numerical algorithm completely avoids the problems caused by the leading-edge singularity leading to a much higher order of accuracy for the numerical solution of the flow in the critical region. Although this method was demonstrated for the leading-edge singularity in the present study, it can directly be applied to deal with various two-dimensional angular singularities and can also be extended to treat three-dimensional problems. The treatment of the singularity proposed is local. Consequently, the algorithm is not limited to any specific finite-discretization scheme.

ACKNOWLEDGEMENTS

The present work received support through the ‘Bavarian Consortium for High-Performance Engineering and Scientific Computing’ (FORTWIHR) and the follow-up consortium ‘Bavarian Network for High-

Performance Engineering and Scientific Computing' (KONWIHR). J.M.S. held a scholarship of the German Academic Exchange Service (DAAD), which is thankfully acknowledged.

REFERENCES

1. Carrier CF, Lin CC. On the nature of the boundary layer near the leading edge of a flat plate. *Quarterly Applied Mathematics* 1948; **6**:63–68.
2. Moffat HK. Viscous and resistive eddies near a sharp corner. *Journal of Fluid Mechanics* 1964; **18**:1–18.
3. Kondratév VA. Asymptotic of solution of the Navier–Stokes equation near the angular point of the boundary. *Journal of Applied Mathematics and Mechanics* 1967; **31**:125–129.
4. Ingham DB, Kelmanson MA. *Boundary Integral Equation Analyses of Singular*, *Potential*, *and Biharmonic Problems*. Springer: Berlin, 1984.
5. Pozrikidis C. *Boundary Integral and Singularity Methods for Linearlized Viscous Flow*. Cambridge University Press: Cambridge, 1991.
6. Georgiou G, Olson L, Schultz W. Singular finite elements for the sudden-expansion and the die-swell problems. *International Journal for Numerical Methods in Fluids* 1990; **10**:357–372.
7. Georgiou G, Olson L, Schultz W. The integrated singular basis function method for the stick-slip and the die-swell problems. *International Journal for Numerical Methods in Fluids* 1991; **13**:1251–1265.
8. Botta EF, Dijkstra D. An improved numerical solution of the Navier–Stokes equations for laminar flow past a semi-infinite flat plate. *Technical Report* TW-80, University of Twente, 1970.
9. Roache PJ. *Computational Fluid Dynamics*. Hermosa: Albuquerque, NM, 1976.
10. Apostolescu V. Numerische Behandlung der stationären Umströmung einer Ecke bei zähen inkompressiblen Fluiden. *Ph.D. Thesis*, Technische Universität München, 1985.
11. Dennis SCR, Qiang W, Coutanceau M, Launay J-L. Viscous flow normal to a flat plate at moderate Reynolds number. *Journal of Fluid Mechanics* 1993; **248**:605–635.
12. Blum H. The influence of re-entrant corners in the numerical approximation of viscous problems. In *Proceedings of Fifth GAMM Seminar*, vol. 24. Vieweg: Brauschweig, 1989; 37–46.
13. Alleborn N, Nandakumar N, Raszillier H, Durst F. Further contributions to the two-dimensional flow in a sudden expansion. *Journal of Fluid Mechanics* 1997; **330**:169–188.
14. Salamon TR, Bornside DE, Armstrong RC, Brown R. The role of surface tension in the dominant balance in the die-swell singularity. *Physics of Fluids* 1995; **7**:2328–2344.
15. Huang H, Seymour R. Finite difference solutions of incompressible flow problems with corner singularities. *Journal on Scientific Computation* 2000; **15**:265–292.
16. Pozrikidis C. Boundary element grid optimization for Stokes flow with corner singularities. *Journal of Fluids Engineering* 2002; **124**:22–28.
17. Floryan JM, Czechowsky L. On the numerical treatment of corner singularity in the vorticity field. *Journal of Computational Physics* 1995; **118**:222–228.
18. Schultz W, Gervasio C. A study of the singularity in the die-swell problem. *Quarterly Journal of Mechanics and Applied Mathematics* 1990; **43**:407–425.
19. Ingham DB, Tang T, Morton BR. Steady two-dimensional flow through a row of flat plates. *Journal of Fluid Mechanics* 1990; **210**:281–302.
20. In KM, Choi DH, Kim MU. Two-dimensional viscous flow past a flat plate. *Fluid Dynamics Research* 1995; **15**:13–24.
21. Ladevèze J, Peyret R. Calcul numérique déune solution avec singulaité des équations de Navier–Stokes: écoulement dans un canal avec variation brusque de section. *Journal de Mécanique* 1974; **13**:367–396.
22. Van Dyke M. *Perturbation Methods in Fluid Mechanics*. Parabolic Press: Stanford, CA, 1975.
23. Shi J-M. Numerical study of classical low Reynolds number flow problems: leading edge singularity of a semi-infinite plate and hot-wire near-wall corrections. *Ph.D. Thesis*, Institute of Fluid Mechanics, Friedrich-Alexander University of Erlangen-Nuremberg, ISBN 3-8322-1037-7, Shaker Verlag: Aachen, 2002.
24. Durst F, Schäfer M. A parallel blockstructured multigrid method for the prediction of incompressible flows. *International Journal for Numerical Methods in Fluids* 1996; **22**:549–565.
25. Demirdžić I, Perić M. Finite volume method for prediction of fluid flow in arbitrary shaped domains with moving boundaries. *International Journal for Numerical Methods in Fluids* 1990; **10**:771–790.
26. Khosla PK, Rubin SG. A diagonally dominant second-order accurate implicit scheme. *Computers and Fluids* 1974; **2**:207–209.
27. Patankar SV, Spalding DB. A calculation procedure for heat, mass and momentum transfer in three-dimensional parabolic flows. *International Journal of Heat and Mass Transfer* 1972; **15**:1787–1806.
28. Stone HL. Iterative solution of implicit approximations of multi-dimensional partial differential equations. *SIAM Journal on Numerical Analysis* 1968; **5**:530–558.
29. Hortmann M, Perić M, Scheuerer G. Finite volume multigrid prediction of laminar natural convection: Bench-mark solutions. *International Journal for Numerical Methods in Fluids* 1990; **11**:189–207.

30. Lange CF, Schäfer M, Durst F. Local block refinement with a multigrid flow solver. *International Journal for Numerical Methods in Fluids* 2002; **38**:21–41.
31. Schlichting H. *Boundary Layer Theory* (7th edn). McGraw-Hill: New York, 1987.
32. Ferziger JH, Perić M. Further discussion of numerical errors in CFD. *International Journal for Numerical Methods in Fluids* 1996; **23**:1–12.
33. Imai I. Second approximation to the laminar boundary-layer flow over a flat plate. *Journal of Aeronautical Sciences* 1957; **24**:155–156.
34. Lewis JA, Carrier GF. Some remarks on the flat plate boundary. *Quarterly of Applied Mathematics* 1949; **7**:228–234.
35. Dean WR. On the steady motion of viscous fluid past a flat plate. *Mathematika* 1954; **1**:143–156.
36. Davies RT. Laminar incompressible flow past a semi-infinite flat plate. *Journal of Fluid Mechanics* 1967; **27**:691–704.
37. Yoshizawa A. Laminar viscous flow past a semi-infinite flat plate. *Journal of the Physical Society of Japan* 1970; **28**:776–779.
38. Goldstein S. Flow of an incompressible viscous fluid along a semi-infinite flat plate. *Technical Report* HE-150-144, Engineering Research Institution, University of California, 1956.

